Multiscale and Multi-Temporal Simulation of Change of Urban Structures in the Subarctic East Siberian Metropolis of Yakutsk

Sébastien Gadal, Mounir Oukhattar, Jūratė Kamičaitytė, Moisei Zakharov, Walid Ouerghemmi, Ismaguil Hanadé Houmma

Chapter 23
Multiscale and Multi-Temporal Simulation of Change of Urban Structures in the Subarctic East Siberian Metropolis of Yakutsk

Sébastien Gadal, Mounir Oukhattar, Jūratė Kamičaitytė, Moisei Zakharov, Walid Ouerghemmi, and Ismaguil Hanadé Houmma

Abstract In the last twenty years, the Metropolis of Yakutsk has experienced significant changes characterised by intense urban growth, densification, and urban structure changes in a complex geographical environment: extremely low temperature during six to seven months, impacts of permafrost dynamics and relative melting, seasonal exposure to ice breakup on the suburban areas. The urban structure and land-use changes conditioned by the urban growth and environmental impacts are analysed at two geographic scales: the meso-urban level with the use of the Landsat-5 TM, Landsat-8 OLI, and Sentinel-2 MSI satellites images covering the period from 2010 to 2020; and at the regional level with the DMSP-OLS PL (1995–2013) and VIIRS-DNB (2015–2020) sensors. The recognition of the urban structures and land use transformations at both scales are based on the use of the combined machine

S. Gadal (✉) · M. Oukhattar · M. Zakharov · W. Ouerghemmi · I. H. Houmma
Aix-Marseille University, CNRS, ESPACE UMR 7300, Aix-en-Provence, France
e-mail: sebastien.gadal@univ-amu.fr

M. Oukhattar
e-mail: mounir.oukhattar@etu.univ-amu.fr

M. Zakharov
e-mail: moisei.zakharov@etu.univ-amu.fr

W. Ouerghemmi
e-mail: walid.ouerg@gmail.com

I. H. Houmma
e-mail: ismaguil.hanade-houmma@etu.univ-amu.fr

M. Zakharov
Department of Ecology and Geography, Institute of Natural Sciences, North-Eastern Federal University, Republic of Sakha-Yakutia, Russia

J. Kamičaitytė
Cultural and Spatial Environment Research Group, Kaunas University of Technology, Kaunas, Lithuania
e-mail: jurate.kamicaityte@ktu.lt

M. Hanzl et al. (eds.), *Urban Morphology versus Urban Redevelopment and Revitalisation*, The Urban Book Series, https://doi.org/10.1007/978-3-031-77752-3_23

learning data processing. The simulations of the urban structures and land use evolutions to 2030 at the meso-urban and regional scales by Markov chain cellular automata give comparable results of the future trends of the Yakutsk metropolis: reduction of vegetation, forests areas (due to forest fires) and agriculture zones; the increase of bare soil, water surfaces and new urban areas.

Keywords Urbanisation forms · Territorial structures · Remote sensing · Geo-simulation · Yakutsk metropolis

23.1 Introduction

The city of Yakutsk, capital of the Republic of Sakha-Yakutia, had around 330,000 inhabitants in 2023. The metropole is characterised by a spatial and territorial dynamic that is unique in the Russian Arctic regions. Since the 1990s, it experienced continuous demographic and urban growth, while many other pioneer and Arctic cities experienced significant demographic decline or became ghost towns (Gadal et al. 2022). During the Soviet period, under the momentum of central Soviet authority, Yakutia, with its vast natural resources, was a pioneering area for the economic development of the Far East (Péné-Annette et al. 2017). This led to a significant demographic and urban growth, with high levels of net emigration from other regions of the USSR (Vinokurova et al. 1994; Sukneva 2021; Fedorova 1998). Demographic dynamics was particularly intensive in the 1970 and 1980s in the regions and towns of the east, south and west of the Sakha-Yakutia Republic, due to the high demand for labour to support mining activities. It accounted for up to 70% of population movements in Yakutia during this period (Fedorova et al. 2003). With the end of the USSR, most of the pioneering towns linked to the extractive economy lost their populations. During the same period, the rural exodus and the process of territorial integration of the urban centres of central Yakutia were the drivers behind the urban growth of the metropolis of Yakutsk.

Managing urban sprawl in metropolitan areas such as the Siberian metropolis of Yakutsk has become a major challenge in recent years. With new perspectives on sustainable urban growth, it is becoming more and more important to design, develop and implement appropriate land use and management practices (Zhao 2010). New approaches to remote sensing and spatial modelling are crucial in providing valuable information for decision-makers and planners to take informed actions. At the current state of knowledge, various methods exist for mapping spatiotemporal changes in the dynamics of land use units and artificial areas (Bhatti and Tripathi 2014; Lo and Choi 2004; Powell et al. 2007). For example, to study the process of urban sprawl, multi-date and multi-sensor analyses have been widely applied (Wilson et al. 2003; Zeng et al. 2005). In addition, urban planners and local stakeholders also use predictive geo-simulation models to estimate changes in urban fabric (Zanganeh Shahraki et al. 2011). However, given the great spatial variability of the processes and factors influencing urban sprawl, there are controversial views in the literature on the

advantages and limitations of each approach. Among the range of factors, according to Zhao (2010) socio-economic characteristics in particular, social attitudes towards residential plots influence, for example, the types of transport networks and land use patterns in peri-urban areas. Similarly, people's travel distances also have a significant influence on urban sprawl (Kenworthy and Laube 1996). The importance of these socio-economic and physical characteristics in understanding the dynamics of urban change has been highlighted in several research studies (Bhatti et al. 2015; Longley and Mesev 2000). Serra et al. (2008) have analysed the importance of the joint and complementary use of biophysical and socio-economic data to study the main factors responsible for land use and land use change in a Mediterranean region. Similarly, another study by Almeida et al. (2005) showed the importance of using urban infrastructure and socio-economic indicators to understand the probability of urban growth. Other factors, such as population growth, employment and the evolution of built-up areas have also been used as important indicators in modelling urban growth (Fulton et al. 2001).

Nevertheless, urban growth is an inevitable process that, if treated meticulously, can be considered an indicator of any region's social and economic development. This study presents a combined machine learning approach to address the variable growth dynamics of urban and peri-urban areas of Yakutsk metropolis in a geo-simulation Markov chain cellular automata model. Four exploratory scenarios are developed based on a different rate of change in land use and land cover (LULC) and different land development conditions. The specific objectives of this study includes (1) time series LULC classification using ISODATA (Iterative Self-Organizing Data Analysis Technique) and Mahalanobis distance for the period of 2010–2020; (2) multi-scale and multi-temporal simulation of different exploratory scenarios and accuracy assessment using actual land changes; (3) prediction of future LULC for 2030 through the modelling approach (Cellular automat Markov chain) designed to examine spatio-temporal LULC dynamics; and (4) temporal analysis of night-time DMSP OLS and VIIRS satellites data to monitor and understand the evolution of urbanisation between 1995, 2020 and to forecast in 2030 in the Yakutsk metropolitan region. The objective is to set up multi-scale analysis and evolution models based on two methodological fields in artificial intelligence based on a combined approach in machine learning. The interest in cognitive terms of this study is to understand the evolutionary processes of urbanisation and metropolisation in a complex geographical environment characterised by an extreme continental subarctic climate (urban territory subjected to negative temperatures for more than 6 months of the year that can reach −55 °C), impacted by global warming with the increase in temperatures, the relative melting of the permafrost (with the problems of constructions, destructions, carbon emissions etc.) and the annual exposure to ice breakup with flooding on peri-urban areas and satellite villages. The spatial analysis integrates data collected in the field materials combined with the LULC modelling for the geo-simulated evolutions of the Yakutsk metropolis.

23.2 The Metropolis of Yakutsk

The study area includes the Yakutsk metropolis with the peri-urbanized metropolitan region of Central Yakutia (Fig. 23.1) located in the subarctic or sharply continental climate zone of Eastern Siberia and in the central part of Yakutia. The number of ~~its~~ inhabitants of Yakutsk (62°05′N 129°45′E) which increased from 192,000 in 1990 to 339,664 in 2020, makes up a little more than a third of the population (35,36%) of the entire Republic of Sakha (Yakutia) (Figs. 23.2 and 23.3). The Yakutsk as city located in the valley and river terraces of Lena River. The total area of the metropolitan region is 52410,59 km^2. It is bordered to the west by Gornyi ulus, to the north by Namsky ulus, to the east by Megino-Khangalassky ulus, and to the south by Khangalas ulus. The territory of the Yakutsk metropolis is a hilly plain located to the north of the Prilenskoe Plateau. The predominant altitudes are about 250 m above sea level (ASL). The absolute maximum of altitude is 286 m ASL and the minimum is about 86 m ASL is located in the Tuymaada Valley. Most of the area of the district is covered by the closed deciduous forest of the boreal taifa (Fig. 23.1). The dominant tree species are larch and Siberian pine, with small plots of other species, such as spruce, birch, aspen, and others. The climate of the metropolis, as well as that of the whole of Central Yakutia, is extreme continental with long and harsh winters (the average temperature in January is about −40° C) and short but hot summers (the average temperature in July is 19° C). There is characteristic low rainfall throughout the year and dry summer.

23.3 Multisensor's Remote Sensing Data for Multi-Scalar Analysis

The dataset used include the Landsat-5 TM, Landsat-8 OLI, and Sentinel-2 MSI images (Table 23.1). The Sentinel-2 MSI image has three spatial resolutions and thirteen spectral bands. Ten spectral bands of Sentinel-2 were used, excluding the coastal aerosol, water vapour, and cirrus bands that have a spatial resolution of 60 m. The other spectral bands have been reorganised into two combinations. The first combination includes only four spectral bands (blue, green, red, and near infrared) at a resolution of 10 m. The second combination consists of six bands (red edge 1 to 4 and two short-wave infrared (SWIR)) at a resolution of 20 m. Seven spectral bands at a resolution of 30 m were used from Landsat 8 OLI Collection 1, excluding the panchromatic and thermal infrared (TIR) bands. The DMSP/OLS (VNIR) and VIIRS DNB night images were chosen to reconstruct all the data allowing the modelling of the evolution processes of urban structures in the metropolis of Yakutsk.

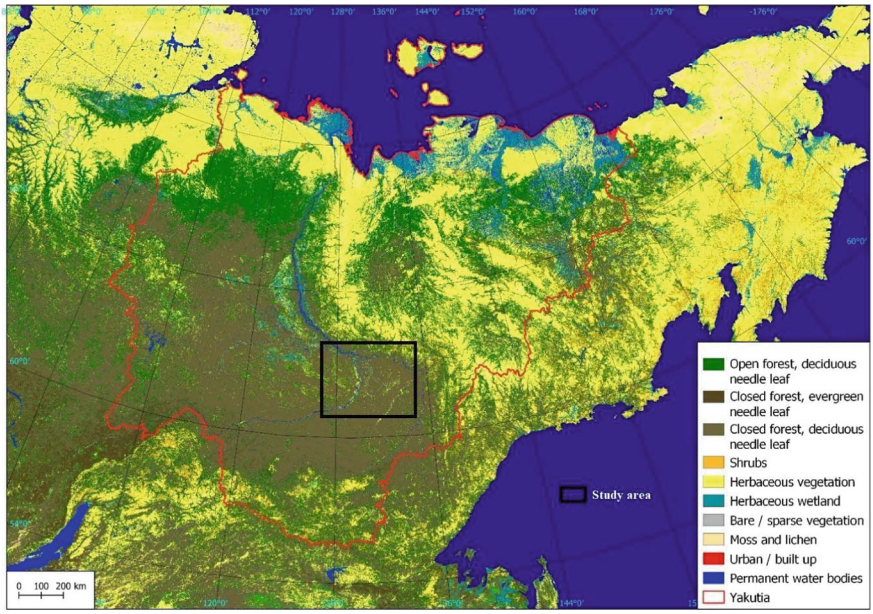

Fig. 23.1 Study area at the scale of the Yakutsk metropolis. (Moisei Zakharov, CNRS ESPACE UMR 7300, 2023) (Buchhorn et al. 2020)

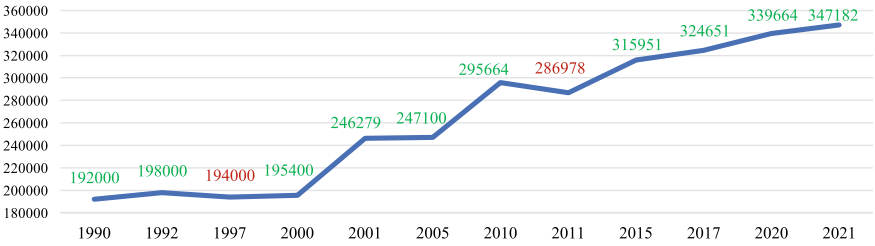

Fig. 23.2 Population evolution in the metropolis of Yakutsk during the period from 1990 to 2021. (Census: https://14.rosstat.gov.ru/chisl_sostav)

23.4 Methodology

The Landsat-5 TM, Landsat-8 OLI series, and Sentinel-2 MSI datasets constitute the geographic-based data used to simulate the urban land use land cover changes in the Yakutsk metropolitan territory until 2030. Regarding the research object, the geo-simulation of the urban growth, and the dominant geographical features of the study area; four classes of land uses were cartography, namely bare soil (unused land and open spaces), urbanisation (residential, commercial, industrial and transport), vegetation (agriculture, trees, shrubs, and meadows) and water bodies (open water, streams, canals, and rivers) (Anderson 1976). Considering the spatial extent

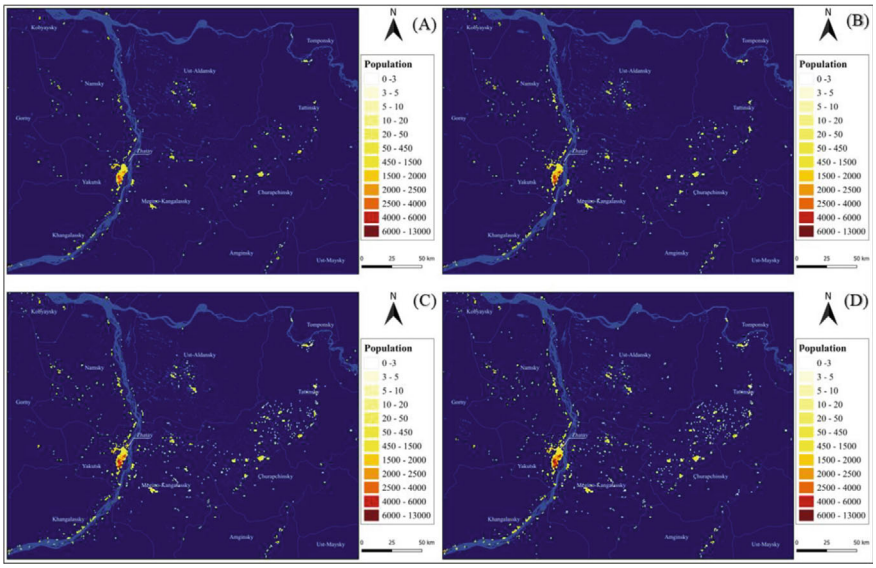

Fig. 23.3 Spatial distribution of the population in the year 2001 (**a**), 2010 (**b**), 2015 (**c**) and 2020 (**d**) using a 100m^2 grid that covers all buildings in the Yakutsk metropolis (Census: https://14.rosstat.gov.ru/chisl_sostav). Sébastien Gadal, Mounir Oukhattar, Moisei Zakharov, Jūratė Kamičaitytė, Walid Ouerghemmi, CNRS ESPACE UMR 7300, 2021

Table 23.1 Satellite data characteristics

Data	Landsat-5 TM	Landsat-8 OLI		Sentinel-2 MSI		DMSP/ OLS	VIIRS DNB
Date of images	2010	2015	2020	2015	2020	1995 to 2013	2015 to 2020
Acquisition date	From 02/ 07/2010 to 31/08/ 2010	From 02/ 07/2015 to 31/08/ 2015	From 02/ 07/2020 to 31/08/ 2020	From 01/ 07/2015 to 31/08/ 2015	From 01/ 07/2020 to 31/08/ 2020	1995 2001 2013	2015 2017 2020
Projection	WGS 84/UTM zone 52N						
Spatial resolution	30–120 m	15−30 m	15−30 m	10−60 m	10−60 m	2,7 km	742 m
Source	USGS. earth explorer					DMSP night-time lights (mines.edu)	VIIRS night-time light (mines.edu)

of the subarctic metropolis of Yakutsk, the subclasses of the four identified land use classes have been aggregated to minimise intra-class confusion. This is aimed at highlighting the forms of the urban structures of the subarctic metropolis of Yakutsk. The approach developed combines three phases of data processing (Fig. 23.4): (1)

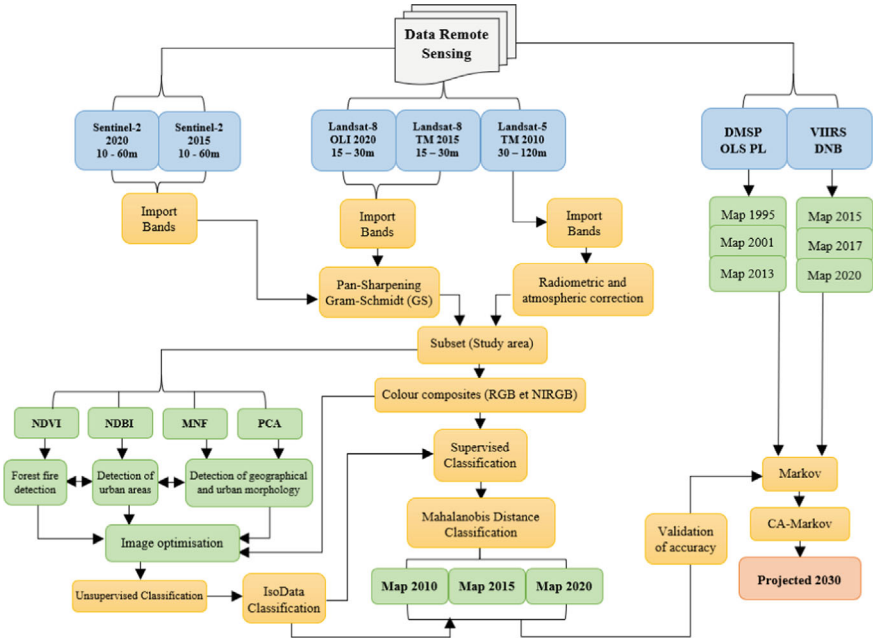

Fig. 23.4 Methodological flowchart

A LULC classification approach that aims to test the best classification algorithm against the diverse types of remote sensing sensors used (Landsat-5 TM, Landsat-8 OLI, and Sentinel-2 MSI) to obtain the LULC maps of 2010, 2015, and 2020. (2) The kappa index and overall accuracy were used for the validation of LULC classification results from Landsat and sentinel-2 data. (3) The CA-Markov cellular automaton simulation was subsequently used to predict the spatial distribution of LULC classes for 2030. Similarly, DMSP and VIIRS nightlight remote sensing images are used for modelling the urban changes in 2030 at the metropolitan region of Yakutsk.

23.4.1 LULC Classification of the Yakutsk Metropolis Areas

Data pre-processing. Atmospheric corrections and radiometric calibration were applied to Landsat-5 TM/8 OLI and Sentinel-2 MSI data. For the Landsat-8 OLI and Sentinel-2 MSI sensors, the RGB and NIR bands were stacked and then cut to cover the study area. Gram-Schmidt's panoramic sharpness (GS) algorithm was applied to resample these images at resolutions of 15 m for Landsat 8 images and 10 m for Sentinel 2 data respectively. Landsat-5 TM data were not resampled at 15 m because they do not contain the panchromatic band.

ISODATA unsupervised classification. The ISODATA clustering algorithm is an improved version of the k-means clustering algorithm (Jensen 2005). The ISODATA algorithm calculates the class averages evenly distributed across the data space and then iteratively groups the remaining pixels using minimum distance techniques. Each iteration recalculates the averages and reclassifies the pixels relative to the new averages. This process continues until the number of pixels in each class changes below the selected pixel change threshold or the maximum number of iterations is reached (Kantakumar and Neelamsetti 2015).

The ISODATA classifier gave the best result after testing algorithms and comparisons of the subarctic metropolis the LULC maps modelled. The classification combines a coloured composition (RGB and NIRGB), indices (NDVI, and NDBI), PCA, and MNF neo-images. This processing step is necessary to filter and merge the best results to have an image optimisation that has achieved high classification accuracy. This step also allowed the identification of the dominant LULC classes in the study area which were subsequently mapped by a supervised classification approach using the Mahalanobis distance algorithm (Fig. 23.4).

Supervised classification by Mahalanobis distance. Mahalanobis distance is a direction-sensitive distance classifier. It uses statistics for each input data class. The Mahalanobis distance is like the maximum probability classification, but it assumes that all class covariances are equal, and therefore, it is a faster method of calculus (Eskandari et al. 2020). During the image processing, no specific distance threshold value was used, allowing the algorithm to rank all pixels at the closest training data (Randazzo et al. 2021). In this study, after testing and visually comparing the LULC results of six supervised classification algorithms (Support Vector Machine, Spectral Angle Mapper, Parallelepiped, Minimum Distance, Maximum Likelihood and Mahalanobis Distance), the Mahalanobis Distance algorithm gave the best-supervised classification result (Table 23.4). The Mahalanobis algorithm was used to classify the four dominant LULC classes in the study area identified by the ISODATA classifier from the coloured compositions (RGB and NIRGB) of the Landsat and Sentinel-2 data (Fig. 23.4).

23.4.2 Prediction of Future LULC Dynamics

The cellular automat Markov (CA-Markov) model was used to predict the LULC change of the Yakutsk metropolis in 2030. CA-Markov is a Change/Time or Environment/Simulation probabilistic model based on the LULC maps generated from the Mahalanobis and ISODATA classifiers. The classified LULC maps for 2010, 2015, and 2020 were used to acquire the dynamic change for the LULC classes between 2010 and 2015, 2015 and 2020 (Klimsiak 2016; Gidey et al. 2017) generating intermediary maps of LULC potential transitions and LULC transition probability matrix from 2010 to 2015, from 2015 to 2020, and 2020 to 2030. Thus, the transient probabilities and adequacy zones are created by running the Markov probabilistic matrix before running the CA-Markov geo-simulation processing (Jazouli et al. 2018).

23.4.3 Evaluation of the Accuracy of the Classification

The LULC maps of 2020 from Landsat-8 OLI and Sentinel-2 MSI have been validated using 2020 RGB "natural" colour composition images from WORLDVIEW-3 satellite with a resolution of 30 cm through visualisation on the Google Earth platform. To do this, 300 ground checkpoints were considered to evaluate the accuracy of the 2020 cartographic results of each classification method (ISODATA and Mahalanobis distance) using the overall accuracy index (OA) and the Kappa coefficient (K). This made it possible to verify and compare the performance of the algorithms in their ability to classify LULC units from Landsat-8 OLI and Sentinel-2 MSI data. The Kappa index and overall accuracy are two indicators that provide information on the synthetic accuracy of all LULC classes. The specific accuracy of each class of LULC is provided by user accuracy (UA) and producer accuracy (PA). These indices are calculated from the following equations (Eqs. 23.1, 23.2, 23.3 and 23.4):

$$UA = \frac{Number\ of\ pixels\ correctly\ classified\ in\ each\ category}{Total\ number\ of\ reference\ pixels\ in\ this\ category(row\ total)} \times 100 \tag{23.1}$$

$$PA = \frac{Number\ of\ correctly\ classified\ pixels\ in\ each\ category}{Total\ number\ of\ pixels\ classified\ in\ this\ category(Total\ column)} \times 100 \tag{23.2}$$

$$OA = \frac{Total\ number\ of\ correctly\ classified\ pixels\ (Diogonal)}{Total\ number\ of\ reference\ pixels} \times 100 \tag{23.3}$$

$$K = \frac{N\sum_{i=1}^{r}(x_{ii}) - \sum_{i=1}^{r}(x_i + Xx_{+1})}{N^2 - \sum_{i=1}^{r}(x_{ii}Xx_{+1})} \tag{23.4}$$

where: $\mathbf{r}$ = number of rows and columns in the error matrix, $\mathbf{N}$ = total number of observations (pixels), $\mathbf{X_{ii}}$ = observation in row i and column i, $\mathbf{X_{i+}}$ = marginal total of row i, and $\mathbf{X_{+i}}$ = marginal total of column i.

23.5 Results and Discussions

23.5.1 LULC Change Analysis

The LULC maps (2010, 2015, 2020 and 2030) obtained by supervised and unsupervised classification of Landsat-5 TM/8 OLI and Sentinel-2 MSI images are presented in Figs. 23.5 and 23.6 respectively. These cartographic results present the current and future changes of four dominant LULC classes of the subarctic metropolis Yakutsk. These mapped LULC classes include 4 types of land use/land cover: bare soil (yellow

colour), vegetation (green colour), water bodies (blue colour) and urbanisation (red colour).

The comparative analysis of the results from these two sensors and by LULC classification methods reveals a difference in the results obtained by supervised and

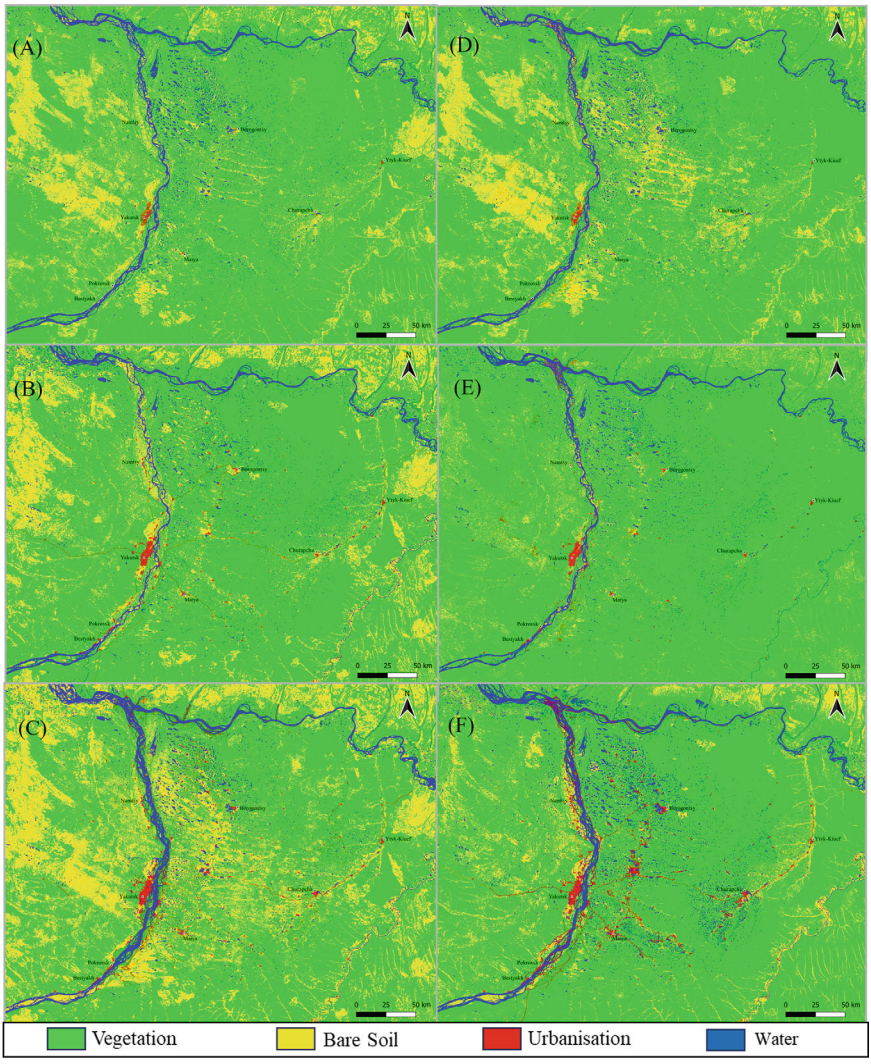

Fig. 23.5 Transformation and geo-simulation of the urban structures of central Yakutia 2015–2020 based on Landsat-5 TM **a**, **b** and Landsat-8 OLI **b**, **d** by ISODATA **a**, **b** and Mahalanobis distance **d**, **e**. Geo-simulation of the urban structures in 2030 by cellular-automat Markov chain **c**, **f**. (USGS earth explorer: https://earthexplorer.usgs.gov/). Sébastien Gadal, Mounir Oukhattar, Moisei Zakharov, Jūratė Kamičaitytė, Walid Ouerghemmi, CNRS ESPACE UMR 7300, 2021

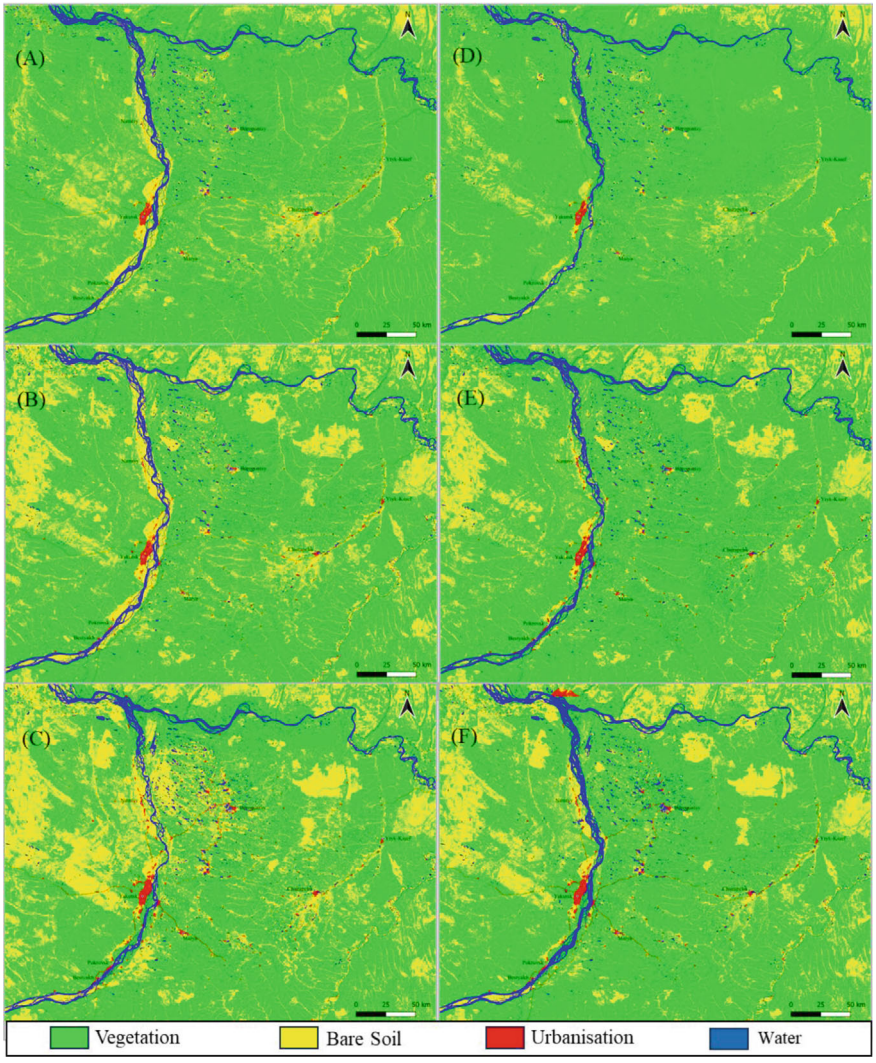

Fig. 23.6 Transformation and geo-simulation of the urban structures of central Yakutia 2015–2020 based on sentinel 2-MSI (**a**) (**b**) (**d**) by ISODATA (**a**) (**b**) and Mahalanobis distance (**d**) (**e**). Geo-simulation of the urban structures in 2030 by cellular-automat Markov chain (**c**) (**f**). (USGS earth explorer https://earthexplorer.usgs.gov/). Sébastien Gadal, Mounir Oukhattar, Moisei Zakharov, Jūratė Kamičaitytė, Walid Ouerghemmi, CNRS ESPACE UMR 7300, 2021

unsupervised classification of the Landsat-8 OLI images of the year 2020. In contrast, the results of these two classification methods show no significant visual difference from Sentinel-2 data. This could be explained by the low performance of the Mahalanobis algorithm compared to the ISODATA algorithm applied on a combination of MNF, NDVI, NDBI, PCA, RGB and NIRGB. Visually, this combination gave

comparable results for both, the 15 m resampled Landsat-8 OLI data and the 10 m resolution Sentinel-2 MSI data. Over the period from 2010 to 2030, the image analysis of the LULC results shows differentiated changes by land use unit type. The main changes and territorial transitions are observed in the bare soil, vegetation, and urbanisation classes.

We can go to see on the results by Sentinel-2, a significant increase in the urbanisation process between 2015 and 2030. The main changes were observed in urban structures (spatial organisation, and densification of the urban fabric). This increase in urbanised areas is accompanied by a growth in bare soil and a decrease in vegetation. This transition could be explained by a strong influence of the human factor (urbanisation) on the occurrence of forest fires in this area (Janiec and Gadal 2020). The number of forest fires in Central Yakutia is 300 cases over the period between 2000 and 2020 or 295,000 hectares with a peak of 1,7 million hectares of burnt area in 2002 (Petrov et al. 2022). Similarly, the denudation of bare soil is related to the process of anthropisation and intense agricultural activities.

The multi-temporal LULC classes change statistical analysis of the Yakutsk subarctic metropolis between 2010 and 2030 (Table 23.2 and Fig. 23.7) illustrates the above-mentioned cartographic results in Figs. 23.5 and 23.6. The analysis of these statistical results highlights a territorial dynamic shown by a process of urbanisation. These spatial and territorial dynamics will increase in the coming years according to the model geo-simulation. All spatial statistics of two classification methods tested on a multi-sensor approach (Landsat-5 TM/8 OLI and Sentinel-2 MSI) show significant development of urban areas.

Referring to the statistics of the unsupervised classification of Landsat-5 TM/8 OLI images (Table 23.2), the urbanised areas evolved from 0,1% (75,5 km^2) in 2010 to 0,4% (215,5 km^2) in 2020 with a positive rate of change of 185,3%. According to the projection in 2030, the urban coverage of the subarctic metropolis would expect 1,8% (946,2 km^2) with a rate of change of 339,1% between 2020 and 2030. This process of the rapid urbanisation of the metropolis could be linked to local demographic dynamics (population migration), natural population growth and the socio-economic development of the region.

On the other hand, the statistics provided in Table 23.2 show both regressive and progressive changes in the LULC natural units of the subarctic metropolis of Yakutsk. While we can see a clear increase in bare soils from 7,5% (3944,8 km^2) in 2010 to 8,9% (4653,5 km^2) in 2020. Vegetation cover has decreased remarkably over the same period. It decreased from 86,3% (45,236,5 km^2) in 2010 to 85,2% (44,638,9 km^2) in 2020. Based on this regressive vegetation trend, the vegetation cover of the area could decrease to 80% (41,943,5 km^2) in 2030 with a negative rate of change of −3,8% according to CA-Markov-based projections.

Similarly, referring to the unsupervised classification statistics of Sentinel-2 MSI images (Table 23.3 and Fig. 23.8), a similar trend of LULC changes is observed. The urbanised areas evolved from 0,04% (18,4 km^2) in 2015 to 0,1% (30,6 km^2) in 2020 with a positive rate of change of 67,3%. The simulations based on CA-Markov show that urbanisation of the subarctic metropolis would reach 0,52% (271,6 km^2) with a rate of change of 780,3% between 2020 and 2030. At the same time, bare soils

Table 23.2 LULC changes of landsat-5 TM/8 OLI between 2010, 2015, 2020 and 2030

LULC types	LULC area								LULC change					
	2010		2015		2020		2030		2010–2015		2015–2020		2020–2030	
	(km^2)	(%)	(km^2)	(%)	(km^2)	(%)	(km^2)	(%)	(km^2)	(%)	(km^2)	(%)	(km^2)	(%)
Unsupervised classification														
Bare soil	3944,8	7,5	1411,1	2,7	4653,5	8,9	5416,2	10,3	−2533,7	−64,2	3242,4	229,8	−237,3	−5,1
Vegetation	45,236,5	86,3	47,472,6	90,6	44,638,9	85,2	41,943,5	80	2236,1	4,9	−2833,8	−6,0	−1695,3	−3,8
Water bodies	3153,5	6,0	3381,7	6,5	2902,7	5,5	4104,7	7,8	228,2	7,2	−479,0	−14,2	1202,0	41,4
Urbanisation	75,5	0,1	145,2	0,3	215,5	0,4	946,2	1,8	69,7	92,3	70,2	48,4	730,7	339,1
Total	52,410,4	100	52,410,6	100	52,410,5	100	52,410,6	100						
Supervised classification														
Bare soil	12,590,8	24,0	7975,2	15,2	3545,0	6,8	15,706,8	30,0	−4615,6	−36,7	−4430,2	−55,5	12,161,8	343,1
Vegetation	36,562,9	69,8	40,996,4	78,2	46,002,4	87,8	31,241,5	59,6	4433,5	12,1	5006,0	9,6	−14,760,9	−32,1
Water bodies	2956,2	5,6	2952,0	5,6	2096,5	4,0	4244,5	8,1	−4,2	−0,1	−855,5	−1,6	2148,0	102,5
Urbanisation	300,2	0,6	486,6	0,9	766,8	1,5	1217,7	2,3	186,4	62,1	280,3	0,5	450,9	58,8
Total	52,410,1	100	52,410,2	100	52,410,8	100	52,410,6	100						

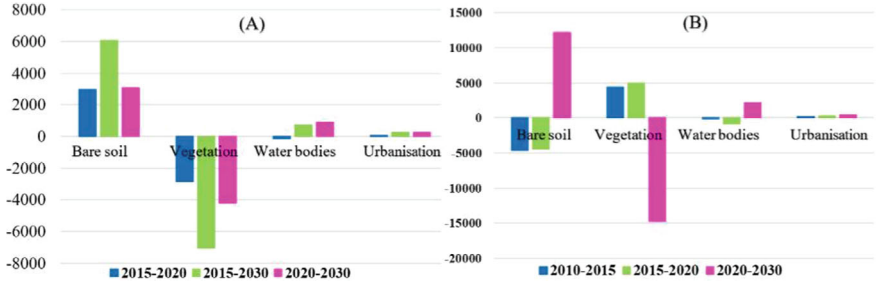

Fig. 23.7 Gain/loss (km^2) of the area by LULC class for the periods: 2010, 2015, 2020 and 2030 of Landsat−5 TM/8 OLI data

increased from 8,4% (4382,9 km^2) in 2015 to 14,6% (7366,3 km^2) in 2020 with a positive rate of change of 68,1%. This evolution would reach 19,9% (10,451,3 km^2) in 2030 with a rate of change of 41,9%.

In contrast, the vegetation class has decreased significantly to 86,6% (45,370,1 km^2) in 2015, 81,2% (42,538,1 km^2) in 2020 and 73,1% (38,322,7 km^2) in 2030. The rate of change is −6,2% between 2015 and 2020 and −9,9% between 2020 and 2030. The reduction in vegetation represented by agricultural and forest areas is correlated to forest fires, urban growth, and the drop in water levels between 2015 and 2020 from 5% (2638,8 km^2) to 4,7% (2475 km^2).

In this analysis of LULC change statistics, the discussion focused on the rates of change provided by unsupervised classification as it is the most accurate for the results from these two sensors (Landsat-5 TM/8 OLI and Sentinel-2 MSI).

23.5.2 Evaluation of the Accuracy of the LULC Classification

The accurate evaluation of the supervised and unsupervised classification images was performed using 300 stratified random points (Table 23.4). As a result of the evaluation of the stratified random points, the Sentinel-2 MSI-derived unsupervised classification LULC images have a higher kappa value (0,93) and overall accuracy (94%) than the Landsat-derived unsupervised classification LULC images which have a kappa value (0,78) and overall accuracy (84%). The Sentinel-2 derived supervised classification LULC images have a higher kappa value (0,85) and overall accuracy (89%) than the Landsat-derived supervised classification LULC images which have a kappa value (0,7) and overall accuracy (77%). Overall, the classified LULC maps have a good matching agreement with a kappa value of 70% and 78% (Landsat) and 85% and 93% (Sentinel-2) respectively for supervised and unsupervised classification. This is only a general assessment. These results may therefore vary depending on the use of different classification methods and statistics for accuracy assessment.

From this evaluation, the classification method based on the ISODATA algorithm applied on a combination of (NDVI, PCA, MNF, NDBI, RGB and NIRGB) gave

Table 23.3 LULC changes of sentinel-2 MSI between 2010, 2015, 2020 and 2030

LULC types	LULC area						LULC change						
	2015		2020		2030		2015–2020		2015–2030		2020–2030		
	(km^2)	(%)	(km^2)	(%)	(km^2)	(%)	(km^2)	(%)	(km^2)	(%)	(km^2)	(%)	
Unsupervised classification													
Bare soil	4382,9	8,4	7366,3	14,1	10,451,3	19,9	2983,3	68,1	6068,4	138,5	3085,1	41,9	
Vegetation	45,370,1	86,6	42,538,1	81,2	38,322,1	73,1	−2831,9	−6,2	−7048	−15,5	−4216,1	−9,9	
Water bodies	2638,8	5	2475	4,7	3365,5	6,4	−163,8	−6,2	726,7	27,5	890,5	36	
Urbanisation	18,4	0,04	30,9	0,06	271,6	0,5	12,4	67,3	253,1	1372,7	240,7	780,3	
Total	52,410,2	100	52,410,2	100	52,410,5	100							
Supervised classification													
Bare soil	5809,5	11,1	12,829,2	24,5	17,257,5	32,9	7019,8	120,8	11,448	197,1	4428,2	34,5	
Vegetation	44,206,7	84,4	37,000	70,6	31,502,9	60,1	−7206,7	−16,3	−12,703,8	−28,7	−5497,1	−14,9	
Water bodies	2371,4	4,52	2536,1	4,84	3566	6,8	164,7	6,95	1194,6	50,4	1029,9	40,6	
Urbanisation	22,87	0,04	45,05	0,09	84,54	0,16	22,18	96,98	61,67	269,7	39,5	87,7	
Total	52,410,4	100	52,410,4	100	52,410,9	100							

Table 23.4 Results of the evaluation of the accuracy of LULC maps

	Landsat-8 OLI LULC				Sentinel-2 MSI LULC			
	Supervised classification		Unsupervised classification		Supervised classification		Unsupervised classification	
	User's accuracy	Producer's accuracy	User's accuracy	Producer's accuracy	User's accuracy	Producer's accuracy	User's accuracy	Producer's accuracy
Bare soil	100%	44%	44%	37%	50%	30%	100%	78%
Vegetation	75%	100%	78%	75%	84%	83%	85%	100%
Water bodies	100%	100%	98%	99%	100%	100%	100%	100%
Urbanisation	46%	100%	70.37%	83%	83%	90%	92%	100%
Overall accuracy	77%		84%		89%		94%	
Kappa coefficient	0,70		0,78		0,85		0,93	

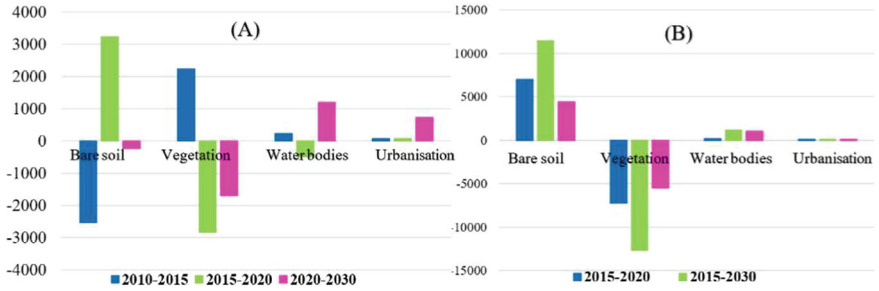

Fig. 23.8 Gain/loss (km^2) of the area by LULC class for the periods: 2010, 2015, 2020 and 2030 of Sentinel-2 data

the best accuracies of LULC classification for both sensors (Landsat-8 OLI and Sentinel-2 MSI). This demonstrates the importance of using an image classification approach combining multispectral transformation techniques (PCA, and MNF), spectral indices (NDVI, NDBI) and colour compositions rather than classification based on a Landsat-8 OLI or Sentinel-2 MSI multispectral raw images. Indeed, the NDVI is used to detect burnt areas, water surfaces, bare soil, and vegetation density and the NDBI is an indice that highlights urban areas where reflectance is higher in the Short-Wave InfraRed spectrum (SWIR) than in the Near InfraRed spectrum (NIR). In addition, to reduce redundancy in the data, the MNF and PCA make it possible to highlight urban morphology (road network, urban fabric, spatial distribution of urban areas) and the geomorphological forms of subsurface structures. The higher specific detection of each of these indices and transformations allows the ISODATA algorithm to easily separate the pixel values of each LULC unit.

23.5.3 Regional Geo-Simulation by NOAA DMSP-OLS and VIIRS-DNB Night-Time Images

The built-up urban areas of the metropolis are recognised and extracted from VIIRS-DNB and DMSP-OLS data for modelling and simulating the urban transformations in 2030 by CA-Markov machine learning processing at the regional scale.

NOAA-DMSP-OLS night-time images. The DMSP/OLS data were used for geo-simulation of urban forms and structural change in the subarctic metropolis of Yakutsk. Figure 23.9 shows built-up dynamics mapped with DMSP/OLS data in1995, 2001 and 2013 and in 2030 by geo-simulation. The image analysis shows an increase in the intensity of night light in the subarctic metropolis of Yakutsk corresponding to urban densification. The highest numerical count values represented by the red colour correspond to the areas of concentration of urbanisation and populations. Between 1995 and 2013 there is a significant spatial increase in urban forms and structures (light intensity of DMSP/OLS data). This expansion will become more

significant in the next seventeen years (2030). The result of the geo-simulation in 2030 confirms the urban and population densification observed between 1995 and 2013. The urban expansion of the subarctic metropolis of Yakutsk would result in 2030 in the expansion of existing urban centres and the appearance of new small urban centres. The territorial urban evolution is corroborated with the evolution of population growth which has evolved from 192 000 in 1990 to 347 182 inhabitants in 2021. Similarly, the geo-simulation result based on DMSP/OLS data supports the projected evolution of urban areas 75,5 km^2 in 2010 to 946,2 km^2 in 2030 derived from the LULC geo-simulation.

VIIRS-DNB night-time images. Figure 23.10 presents the cartographic result of the dynamics of urban structures from 2015 to 2030 derived from VIIRS DNB night light data at the scale of the Yakutsk metropolis. This cartographic result further confirms the process of increasing urbanisation evolution highlighted by the multi-temporal mapping of DMSP/OLS data and spatial modelling of population evolution (Figs. 23.3 and 23.9). The analysis of the results in Fig. 23.10 indicates nuances in light intensity between years in the centre of the Yakutsk municipality. At this level, the night light intensity VIIRS DNB is represented by two colours (yellow and orange) on the map Fig. 23.10a of 2015 and three levels of assorted colours (yellow, orange, and red) on the maps Fig. 23.10b, c and d of the years 2017, 2020 and 2030. The appearance of the red colour (maximum values of DN) demonstrates the increase in urban density in the centre of the urban municipality of Yakutsk and Zhatay. The

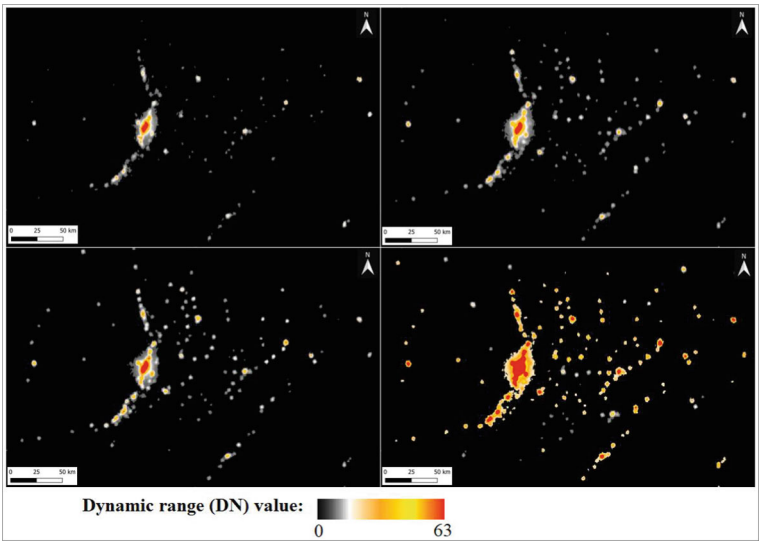

Fig. 23.9 Transformation and geo-simulation of the urban structures of central Yakutia 1995–2030 based on DMSP-OLS VNIR satellite night-time images at the scale of Yakutsk metropolis from 1995 (**a**), 2001 (**b**), 2013 (**c**) and projected in 2030 (**d**). (NOAA: https://ngdc.noaa.gov/eog/dmsp/downloadV4composites.html). Sébastien Gadal, Mounir Oukhattar, CNRS ESPACE UMR 7300, 2022

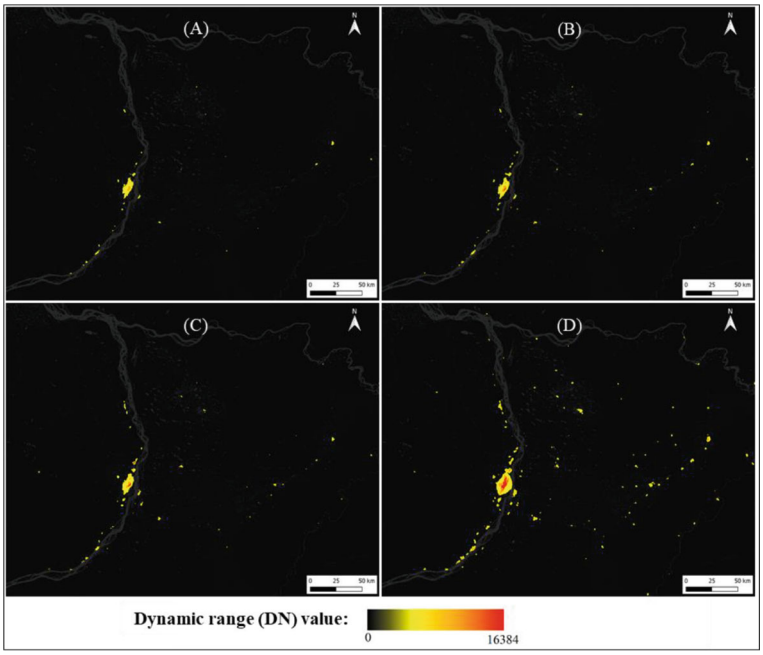

Fig. 23.10 Transformation and geo-simulation of the urban structures of central Yakutia 1995–2030 based on VIIRS-DNB satellite night-time images at the scale of Yakutsk metropolis from 2015 (**a**), 2017 (**b**), 2020 (**c**) and projected 2030 (**d**). (NOAA: ftp://ftp-npp.class.ngdc.noaa.gov/). Sébastien Gadal, Mounir Oukhattar, CNRS ESPACE UMR 7300, 2022

CA-Markov chain simulations in 2030 underpin a process of more important urban densification in the coming years which confirms the dynamics observed between 2015 and 2020.

The spatial organisation of urban structures and the spatial distribution of population density (Fig. 23.3) show a higher concentration in the centre of Yakutsk. The population density in the centre of the municipality ranges from 2500 to 13,000 inhabitants, whereas it varies from about 3 to 2000 inhabitants in the rest of the metropolis. In general, the spatial pattern of the urban development process of the Yakutsk metropolis follows the morphology of the Lena River with a spatial distribution more concentrated in the eastern part than in the western part of Yakutsk city.

23.6 Conclusion

The spatial and structural modelling of evolutions and changes of the subarctic metropolis of Yakutsk over the next 10 years is fundamental regarding the socio-environmental issues due to global warming and the rapid processes of territorialisation with the increase of population and suburbanisation. In this study, an approach to identify the best LULC classification algorithm was applied on Landsat-5 TM/8 OLI and Sentinel-2 MSI multispectral data. In addition, to refine the results from the multi-temporal approach, DMSP/OLS and VIIRS DNB night-time data were used to map and simulate the evolution of urban structures in the metropolis in 2030 at the regional scale. The study revealed that the trajectory changes of the Yakutsk subarctic metropolis are following the morphologic dynamics observed since the end of the 1990s. This form of territorialisation dynamic is intricately linked to a rapid increase in the population, which has risen from 192,000 inhabitants in 1990 to 347,182 inhabitants in 2021. The cartographic and statistical analysis and the CA-Markov chain simulations in 2030 show a good correspondence with the evolution of the spatial distribution of the population between 2001 and 2020. Furthermore, the LULC change analysis showed a continuous increase in urbanisation of 22,9 km^2 in 2015, 45,1 km^2 in 2020 and 84,5 km^2 in 2030. The increase of the road infrastructures and the buildings of the bridge crossing the Lena River will accelerate the trajectory of the morphologic change observed. However, the impact of global warming on permafrost melting is not considered yet. But the impacts are limited because of the technics of building and the limited impacts on soil dynamics. The impacts on the landscape's changes can be significant (Zakharov et al. 2021). According to the satellite sensors, the level of accuracies of the LULC modelling and CA-Markov chain simulations is up from 77% by Landsat-5 TM/8 OLI to 94% with Sentinel-2 MSI. The implementation of oriented object knowledge in the simulation model decreases the level of accuracy performances of the CA-Markov chain simulations: the reasons can be related to the probabilistic model itself, and the type of knowledge and surveys.

Acknowledgements This research was supported by the French National Research Agency (ANR) through the Polar Urban Centers (PUR) project (ANR-14-CE22- 0015), the CNES TOSCA AIM-CEE (Contribution of Multi-Sensor Satellite Imaging to respond to Environmental and Societal issues of Urban Socio-Systems), the CNES TOSCA TRISHNA URBAIN, and the FMSH-RSF research program Human Security in the Russian Arctic Zone.

References

Almeida De CM, Monteiro AMV, Camara G, Soares, Filho BS, Cerqueira GC (2005) GIS and remote sensing as tools for the simulation of urban land use change. Int J Remote Sens 26(4):759–774

Anderson JR (1976) A land use and land cover classification system for use with remote sensor data, vol 964. US Government Printing Office, Washington DC

Bhatti SS, Tripathi NK (2014) Built-up area extraction using Landsat 8 OLI imagery. Giscience & Remote Sens 51(4):445–467
Bhatti SS, Tripathi NK, Nitivattananon V, Rana IA, Mozumder C (2015) A multi-scale modeling approach for simulating urbanization in a metropolitan region. Habitat Int 50(12):354–365
Buchhorn M, Lesiv M, Tsendbazar NE, Herold M, Bertels L, Smets B (2020) Copernicus global land cover layers-collection 2. Remote Sensing 12(108)
Eskandari S, Reza JM, Oliva P, Ghorbanzadeh O, Blaschke T (2020) Mapping land cover and tree canopy cover in Zagros forests of Iran: application of sentinel-2, google earth, and field data. Remote Sens 12(12):1912
Fedorova EN (1998) Naselenie Jakutii: proshloe i nastojashhee (geodemograficheskoe issledovanie) [The population of Yakutia: past and present (geodemographic study)]. Novosibirsk: Nauka Publ 207
Fedorova SA, Bermisheva MA, Villems R, Maksimova NR, Khusnutdinova EK (2003) Analysis of mitochondrial DNA haplotypes in Yakut population]. Mol Biol 37(4):643–653
Fulton W, Pendall R, Nguyen M, Harrison A (2001) Who sprawls most? How growth patterns differ across the US. http://www.brookings.edu/~/media/research/files/reports/2001/7/metropolitanpolicyfulton/fultoncasestudies.pdf
Gadal S, Zakharov M, Kamičaitytė J (2022) Territorialisation, urbanisation, and economic development in the Russian arctic: energy issues. Valery I. Salygin. Energy of the Russian Arctic. Ideals and Realities, Springer Nature Singapore, pp 441–458
Gidey E, Dikinya O, Sebego R (2017) Cellular automata and Markov chain (CA_Markov) model-based predictions of future land use and land cover scenarios (2015–2033) in Raya, northern Ethiopia. Model Earth Syst Environ 3:1245–1262
Janiec P, Gadal S (2020) A comparison of two machine learning classification methods for remote sensing predictive modeling of the forest fire in the North-Eastern Siberia. Remote Sens 12(24):4157
El Jazouli A, Barakat A, Khellouk R, Rais J, El Baghdadi M (2018) Remote sensing and GIS techniques for prediction of land use land cover change effects on soil erosion in the high basin of the Oum Er Rbia river (Morocco). Remote Sens Appl: Soc Environ 13:361–374
Jensen JR (2005) Introductory digital image processing: a remote sensing perspective, 3rd edn. Pearson Prentice Hall, Upper Saddle River
Kantakumar LN, Neelamsetti P (2015) Multi-temporal land use classification using hybrid approach. Egypt J Remote Sens Space Sci 18(2):289–295
Kenworthy JR, Laube FB (1996) Automobile dependence in cities: an international comparison of urban transport and land use patterns with implications for sustainability. Environ Impact Assess Rev 16(4–6):279–308
Klimsiak T (2016) Right Markov processes and systems of semilinear equations with measure data. Potential Anal 44(2):373–399
Lo CP, Choi J (2004) A hybrid approach to urban land use/cover mapping using Landsat 7 enhanced thematic mapper plus (ETMþ) images. Int J Remote Sens 25(14):2687–2700
Longley PA, Mesev V (2000) On the measurement and generalisation of urban form. Environ Plan A 32(3):473–488
Péné-Annette A, Gadal S, Kamicaityte-Virbasiene J (2017) Pioneering cities of mining: comparison of the eastern Venezuela and eastern Siberia. Antonio Angelo Martins da Fonseca, Antonio Puentes, Brais Estévez Vilariño. Digit Cities Spat Justice 135–145
Petrov MI, Fedorov AN, Konstantinov PY, Argunov RN (2022) Variability of permafrost and landscape conditions following forest fires in the Central Yakutian Taiga zone. Land 11(4):496
Powell R, Roberts DA, Dennison PE, Hess L (2007) (2007) Sub-pixel mapping of urban land cover using multiple endmember spectral mixture analysis: Manaus, Brazil. Remote Sens Environ 106(2):253–267
Randazzo G, Cascio M, Fontana M, Gregorio F, Lanza S, Muzirafuti A (2021) Mapping of sicilian pocket beaches land use/land cover with sentinel-2 imagery: a case study of Messina province. Land 10(7):678

Serra P, Pons X, Sauri D (2008) Land-cover and land-use change in a Mediterranean landscape: a spatial analysis of driving forces integrating biophysical and human factors. Appl Geogr 28(3):189–209

Sukneva SA (2021) Migration processes in the Sakha republic (Yakutia). Espace populations sociétés

Vinokurova TZ, Shurgina AI, Zheleznova GA (1994) Demograficheskaja situacija v Respublike Saha (Jakutija): problemy i perspektivy [The demographic situation in the Republic of Sakha (Yakutia): problems and prospects], Jakutsk: JaNC SO RAN 72

Wilson JS, Clay M, Martin E, Stuckey D, Vedder-Risch K (2003) Evaluating environmental influences of zoning in urban ecosystems with remote sensing. Remote Sens Environ 86(3):303–321

Zakharov M, Gadal S, Danilov Y, Kamičaitytė J (2021) Mapping Siberian arctic mountain permafrost landscapes by machine learning multi-sensors remote sensing: example of Adycha river valley. In: 7th international conference on geographical information systems theory, applications and management (GISTAM 2021), INSTICC, online streaming, Czech Republic. pp 125–133. ffhal-03207301

Zanganeh Shahraki S, Sauri D, Serra P, Modugno S, Seifolddini F, Pourahmad A (2011) Urban sprawl pattern and land-use change detection in Yazd, Iran. Habitat Int 35(4):521–528

Zeng H, Sui DZ, Li S (2005) Linking urban field theory with Gis and remote sensing to detect signatures of rapid urbanization on the landscape: toward a new approach for characterizing urban sprawl. Urban Geogr 26(5):410–434

Zhao P (2010) (2010) Sustainable urban expansion and transportation in a growing megacity: consequences of urban sprawl for mobility on the urban fringe of Beijing. Habitat Int 34(2):236–243